Subsurface oxide plays a critical role in CO_2 activation by Cu(111) surfaces to form chemisorbed CO_2, the first step in reduction of CO_2

Marco Favaro[a,b,c,1], Hai Xiao[d,e,1], Tao Cheng[d,e], William A. Goddard III[d,e,2], Junko Yano[a,f,2], and Ethan J. Crumlin[b,2]

[a]Joint Center for Artificial Photosynthesis, Lawrence Berkeley National Laboratory, Berkeley, CA 94720; [b]Advanced Light Source, Lawrence Berkeley National Laboratory, Berkeley, CA 94720; [c]Chemical Sciences Division, Lawrence Berkeley National Laboratory, Berkeley, CA 94720; [d]Joint Center for Artificial Photosynthesis, California Institute of Technology, Pasadena CA 91125; [e]Materials and Process Simulation Center, California Institute of Technology, Pasadena CA 91125; and [f]Molecular Biophysics and Integrated Bioimaging Division, Lawrence Berkeley National Laboratory, Berkeley, CA 94720

Contributed by William A. Goddard III, May 9, 2017 (sent for review January 26, 2017; reviewed by Charles T. Campbell and Bruce E. Koel)

A national priority is to convert CO_2 into high-value chemical products such as liquid fuels. Because current electrocatalysts are not adequate, we aim to discover new catalysts by obtaining a detailed understanding of the initial steps of CO_2 electroreduction on copper surfaces, the best current catalysts. Using ambient pressure X-ray photoelectron spectroscopy interpreted with quantum mechanical prediction of the structures and free energies, we show that the presence of a thin suboxide structure below the copper surface is essential to bind the CO_2 in the physisorbed configuration at 298 K, and we show that this suboxide is essential for converting to the chemisorbed CO_2 in the presence of water as the first step toward CO_2 reduction products such as formate and CO. This optimum suboxide leads to both neutral and charged Cu surface sites, providing fresh insights into how to design improved carbon dioxide reduction catalysts.

CO_2 reduction | suboxide copper | ambient pressure XPS | density functional theory | M06L

The discovery of new electrocatalysts that can efficiently convert carbon dioxide (CO_2) into liquid fuels and feedstock chemicals would provide a clear path to creating a sustainable hydrocarbon-based energy cycle (1). However, because CO_2 is highly inert, the CO_2 reduction reaction (CO_2RR) is quite unfavorable thermodynamically. This makes identification of a suitable and scalable catalyst an important challenge for sustainable production of hydrocarbons. We consider that discovering such a catalyst will require the development of a complete atomistic understanding of the adsorption and activation mechanisms involved. Here the first step is to promote initiation of reaction steps.

Copper (Cu) is the most promising CO_2RR candidate among pure metals, with the unique ability to catalyze formation of valuable hydrocarbons (e.g., methane, ethylene, and ethanol) (2). However, Cu also produces hydrogen, requires too high an overpotential (>1 V) to reduce CO_2, and is not selective for desirable hydrocarbon and alcohol CO_2RR products (2). Despite numerous experimental and theoretical studies, there remain considerable uncertainties in understanding the role of Cu surface structure and chemistry on the initial steps of CO_2RR activity and selectivity (3, 4). To reduce CO_2 to valuable hydrocarbons, a source of protons is needed in the same reaction environment (2), with water (H_2O) the favorite choice. Thus, H_2O is often the solvent for CO_2RR, representing a sustainable pathway toward solar energy storage (1). However, we lack a comprehensive understanding of how CO_2 and H_2O molecules adsorb on the Cu surface and interact to first dissociate the CO_2 (5, 6). An overview of the various surface reactions of CO_2 on Cu(111) is reported in Fig. 1, illustrating the transient carbon-based intermediate species that may initiate reactions.

Previous studies using electron-based spectroscopies observed physisorption of gas-phase g-CO_2 at 75 K, whereas a chemisorbed form of CO_2 was stabilized by a partial negative charge induced by electron capture ($CO_2^{\delta-}$) (Fig. 1*A*) (7, 8). The same experiments showed that no physisorption is observed upon increasing the temperature of the Cu substrate to room temperature (r.t.) (298 K) (Fig. 1*B*). Previous ex situ studies performed in ultrahigh vacuum (UHV) (about 10^{-9} Torr) after relatively low CO_2 exposures [from a few to hundreds of Langmuir (L)] at temperatures between 100 K and 250 K did not reveal CO_2 adsorption or dissociation on clean Cu(100) (9), Cu(110) (10), and Cu(111) (11). However, Nakamura et al. (12) showed that when the exposure is increased to sensibly higher values (pressures ranging between 65 Torr and 1,300 Torr for hundreds of seconds), a nearly first-order dissociative adsorption of CO_2 on clean Cu(110) can be detected between 400 K and 600 K (with an activation energy of about 67 kJ·mol^{-1}), according to the reaction $CO_{2,g} \rightarrow CO_g + O_{ads}$ (where O_{ads} stands for surface adsorbed oxygen). A similar phenomenology was also observed by Rasmussen et al. (9) on clean Cu(100) for CO_2 pressures of about 740 Torr and temperatures in the range of 475–550 K (finding an activation energy of about 93 kJ·mol^{-1}). On the other hand, a recent study by Eren et al. (13) performed at much lower CO_2 partial pressures (between 0.05 Torr and 10 Torr) revealed that CO_2 can dissociatively adsorb on Cu(100) and Cu(111) with the consequent formation of surface oxygen as well. Indeed it has been suggested that the CO_2 might dissociate more easily on preoxidized Cu surfaces (3), but there is little evidence to support this important concept. Activation of CO_2 via assumed chemisorbed CO_2 species was reported also on Cu stepped surfaces (11, 14), but direct in situ proof of the existence of such species on Cu(111) is lacking. These uncertainties and discrepancies indicate the importance of

Significance

Combining ambient pressure X-ray photoelectron spectroscopy experiments and quantum mechanical density functional theory calculations, this work reveals the essential first step for activating CO_2 on a Cu surface, in particular, highlighting the importance of copper suboxide and the critical role of water. These findings provide the quintessential information needed to guide the future design of improved catalysts.

Author contributions: M.F., H.X., T.C., W.A.G., J.Y., and E.J.C. designed research, performed research, analyzed data, and wrote the paper.

Reviewers: C.T.C., University of Washington; and B.E.K., Princeton University.

The authors declare no conflict of interest.

Freely available online through the PNAS open access option.

[1]M.F. and H.X. contributed equally to this work.

[2]To whom correspondence may be addressed. Email: wag@wag.caltech.edu, JYano@lbl.gov, or ejcrumlin@lbl.gov.

This article contains supporting information online at www.pnas.org/lookup/suppl/doi:10.1073/pnas.1701405114/-/DCSupplemental.

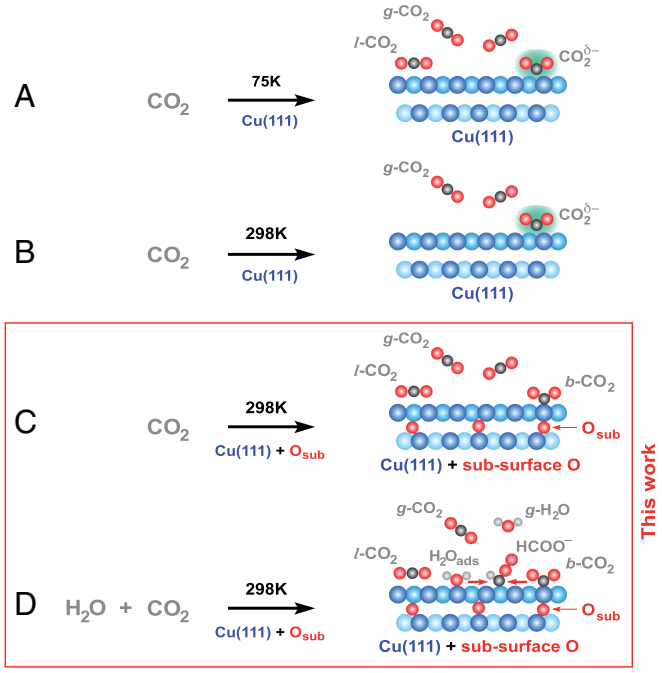

Fig. 1. Overview of surface reactions of CO_2 on Cu(111) under various in situ conditions. Here the *g*-CO_2 indicates gas-phase CO_2, *l*-CO_2 indicates linear (physisorbed) CO_2, and *b*-CO_2 indicates bent (chemisorbed) CO_2. (*A* and *B*) The forms of absorbed CO_2 on pristine Cu(111). (*A*) Both physisorbed *l*-CO_2 and $CO_2^{\delta-}$ are observed at 75 K for pressures up to 10^{-6} Torr. (*B*) Only $CO_2^{\delta-}$ is observed at 298 K for pressures ranging from 10^{-6} Torr to 0.1 Torr. (*C*) The adsorption of CO_2 when a subsurface oxide structure is deliberately incorporated into Cu(111) but without additional H_2O. In this work we observe that a subsurface oxide coverage of about 0.08 ML is responsible for stabilizing *l*-CO_2 at 298 K and 0.7 Torr. Here O_{sub} indicates subsurface oxygen between the top two layers of Cu. (*D*) The cooperative interaction of codosed CO_2 and H_2O on Cu(111) composed of 0.08 ML of subsurface oxide, leading to the first reduction step of CO_2 by adsorbed H_2O_{ads}; HCOO− indicates adsorbed formate.

determining the initial species formed while exposed to realistic gas pressures of CO_2 and H_2O (13, 15).

To advance this understanding, we investigated in detail the initial steps of CO_2 adsorption both alone and in the presence of H_2O on Cu(111) and suboxide surfaces ($Cu_{x=1.5,2.5}O$) via in situ probing of the electronic structure of the surface and reaction products, using ambient pressure X-ray photoelectron spectroscopy (APXPS) performed with soft X-rays (200–1,200 eV) at the solid/gas interface. These studies are complemented with molecular structures and binding free energies of the reaction products at the M06L level (16) of density functional theory (DFT) that was optimized for molecular clusters and reaction barriers. This combination of experiments and calculations allows us to conclude that the presence of suboxide species below the Cu surface and the presence of H_2O play a crucial role in the adsorption and activation of CO_2 on Cu (Fig. 1). Specifically, the presence of subsurface oxygen leads to a specific interaction with gas-phase CO_2 that stabilizes a physisorbed linear CO_2 configuration (*l*-CO_2, Fig. 1*C*). In addition, H_2O in the gas phase (*g*-H_2O), aided by small amounts of suboxide, drives CO_2 adsorption through the transition from the linear physisorbed state to a bent chemisorbed species (*b*-CO_2), which with the aid of H_2O promotes the initial reduction of CO_2 to formate (HCOO−, Fig. 1*D*).

The Cu surface exposing mainly the Cu(111) orientation was prepared in situ from a polycrystalline sample, by repeated argon (Ar) sputtering (normal incidence, 2 keV, 45 min) and annealing cycles in hydrogen (0.15 Torr) at 1,100 K (for 60 min), to obtain a typical 1×1 reconstruction as shown by the low-energy electron diffraction (LEED) pattern in Fig. 2*A* (17). Scanning electron microscopy (SEM) measurements Fig. 2*A* determine that this sputtering and annealing procedure leads to crystalline regions with tens of micrometers mean sizes. The characterized sample surface location remained unchanged throughout the APXPS experiments. The collected spectra were averaged over a beam spot size of ∼0.8 mm in diameter. Although we cannot exclude possible contributions from the presence of grain boundaries, averaging the data over the large probed area led to an eventual grain boundary contribution less than 1% of the overall measured signal, which is below the detection limit. Therefore, their physical/chemical features were not captured in the spectra and do not constitute the focus of this study.

During the APXPS experiments (Fig. 2*B*) performed at r.t. (298 K), CO_2 was first introduced at 0.7 Torr on the pristine metallic Cu(111) surface. For the other experimental conditions and investigated surfaces (see Table 1 and *Supporting Information* for further details), the CO_2 partial pressure ($p(CO_2)$) was kept at 0.35 Torr whereas the total pressure (p_{tot}) was kept constant at 0.7 Torr by codosing H_2O. The APXPS measurements were performed while dosing CO_2 on both metallic Cu(111) and $Cu_{x=1.5}O$ surfaces, whereas CO_2 and H_2O were codosed on metallic Cu(111), $Cu_{x=1.5}O$, and $Cu_{x=2.5}O$ suboxide surfaces (18). The sample surface was clean and no evident C- or O-based contaminations were observed after the cleaning procedure, as shown in Fig. S1. In addition, the in situ mass analysis of the reactants (O_2, CO_2, and H_2O), using a conventional quadrupole mass spectrometer (QMS) mounted on the analysis chamber (and operating at a partial pressure of about 10^{-6} Torr), did not reveal CO cross-contaminations of the gases. However, Fig. S2 shows that, concomitantly with the gas dosing

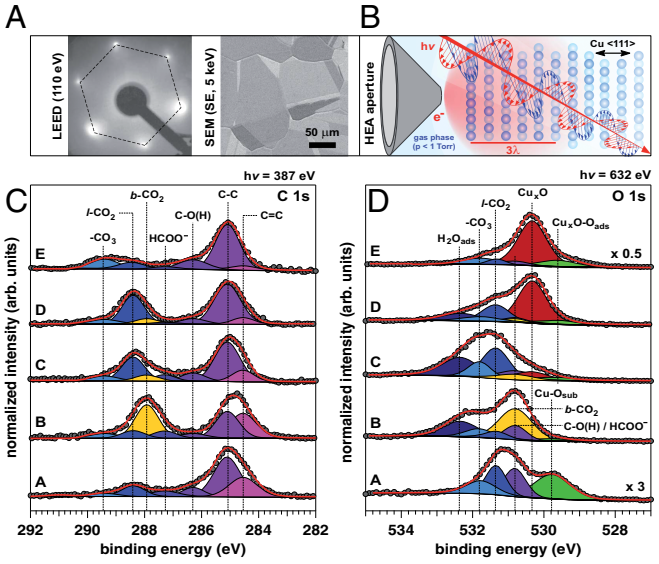

Fig. 2. Investigation of various Cu surfaces using APXPS. (*A*) LEED pattern obtained at an electron kinetic energy of 110 eV and SEM micrograph of the Cu surface after sputtering and annealing cycles obtained by detecting the secondary electrons (SE) with a kinetic energy of the primary beam of 5 keV. (*B*) Schematic of the APXPS measurements with the highlighted probed volume (3λ) along the (111) direction. (*C* and *D*) C 1s and O 1s photoelectron peaks and multipeak fitting results obtained for the various experimental conditions and investigated surfaces (at r.t., 298 K): (experimental condition A) pure CO_2 0.7 Torr on metallic Cu(111); (experimental condition B) $CO_2 + H_2O$ 0.7 Torr on metallic Cu(111); (experimental condition C) $CO_2 + H_2O$ 0.7 Torr on $Cu_{x=2.5}O$; (experimental condition D) $CO_2 + H_2O$ 0.7 Torr on $Cu_{x=1.5}O$); and (experimental condition E) pure CO_2 0.7 Torr on $Cu_{x=1.5}O$. The experimental conditions are summarized in Table 1.

Table 1. Various Cu surface structures and experimental conditions explored with APXPS

Experimental condition	Surface structure	Gas environment	Total pressure, Torr	Temperature, K
A	Metallic Cu(111)	CO_2	0.7	298
B	Metallic Cu(111)	$CO_2 + H_2O$ (1:1)	0.7	298
C	$Cu_{x=2.5}O$	$CO_2 + H_2O$ (1:1)	0.7	298
D	$Cu_{x=1.5}O$	$CO_2 + H_2O$ (1:1)	0.7	298
E	$Cu_{x=1.5}O$	CO_2	0.7	298

(for pressures exceeding 10^{-6} Torr), uptake of carbon contaminations readily occurred [the corresponding binding energy (BE) being centered at 285.1 eV]. Therefore, we cannot completely exclude eventual side reactions and interplay between carbon contaminations and the copper surface.

To understand how interactions between the catalyst surface and CO_2 determine the mechanisms of the initial CO_2 reduction steps, we established the experimental conditions under which a chemisorbed CO_2 state can be stabilized. This provides the basis for tailoring novel catalysts with improved electrochemical performance toward the CO_2RR.

Previously it was difficult to probe these early steps experimentally because r.t. studies require pressures of CO_2 high enough to stabilize a physisorbed configuration sufficiently to allow detailed investigations of various adsorption dynamics, but this high-pressure gas makes it difficult to use electron-based spectroscopies. Our use of APXPS overcomes this difficulty (19–21). To discriminate between physisorbed and chemisorbed CO_2, we monitor the spectral BE shifts of the corresponding C 1s and O 1s photoelectron peaks as a function of the different surfaces and experimental conditions. Physisorption mediated by weak van der Waals (vdW) interactions [surface binding energies of a few millielectronvolts, comparable to $k_B T = 25.7$ meV at 298 K (7)] generally leaves the adsorbate electronic structure unchanged compared with its gas-phase configuration (7, 22–24). In contrast, the chemical bonding needed to form chemisorbed CO_2 on the Cu surface redistributes the electronic density in the adsorbate, leading to appreciable BE shifts compared with the physisorbed state (8).

The adsorption state of CO_2 and the overall surface chemistry of the various systems were monitored by multipeak deconvolution on both the C 1s and O 1s photoelectron spectra (Fig. 2 *C* and *D*), using chemically shifted components sensitive to the initial state effects. Fig. S3 *A* and *B* reports the integrated peak areas of the chemically shifted components for C 1s and O 1s deconvolution, respectively, normalized by the total area underneath the spectra. C 1s and O 1s photoelectron spectra were acquired under APXPS conditions at photon energies of 387 eV and 632 eV, respectively. Because the kinetic energy of the escaping C 1s and O 1s photoelectrons is about 100 eV, the probed depth, 3λ (λ is the electron mean free path) is about 1.2 nm, from the topmost layer (Fig. 2*B*).

The deconvoluted C 1s spectra (see *Supporting Information* for further details) exhibit two main spectral regions: (*i*) At low BE we see chemical species that can be assigned as graphitic carbon (284.5 eV), sp^3 (C-C) carbon (285.2 eV), and C-O(H) bonds (286.3 eV), based on the literature values (15). (*ii*) At higher BE we see spectral fingerprints of higher oxidized carbon structures and adsorbed CO_2, where deconvolution of the spectra indicates the presence of formate (HCOO−) (287.3 eV), chemisorbed (denoted b-CO_2 for bent), and physisorbed CO_2 (denoted l-CO_2 for linear) (287.9 eV and 288.4 eV, respectively) and carbonate ($-CO_3$) (289.4 eV) (15). Finally, a sharp peak centered at about 293.3 eV corresponds to the photoelectron emission of g-CO_2 (Fig. S4).

To disentangle the role of oxygen on the surface and subsurface regions, we carried out a similar analysis on O 1s core-level spectra (Fig. 2*D*). The analysis performed on C 1s was used to help the interpretation of the O 1s spectral envelope while also accounting for the different relative abundances. As with C 1s, we partition the O 1s spectral window into three regions. At low BEs we identify the states of O bonded as follows: (*i*) surface adsorbed O (Cu-O_{ads})on metallic Cu and on suboxidic Cu_xO structures (Cu_xO-O_{ads}) at 531.0 eV and 529.6 eV, respectively (15, 25–27); (*ii*) subsurface adsorbed O (O_{sub}) on metal Cu (Cu-O_{sub}) at 529.8 eV (27) (as we discuss in a later section, such a presence of suboxide plays an important role in stabilizing the l-CO_2); and (*iii*) for $Cu_{x>1}O$ the O 1s is centered at 530.3 eV (15, 18, 25). It is noteworthy that O_{ads} groups on the Cu surface can serve as nucleation sites for hydroxylation when in the presence of H_2O. However, the detection of eventual Cu-OH groups via photoelectron chemical shift identification is complicated by the fact that in the same spectral range (530.6–530.8 eV) several oxygen-based species overlap (such as formate, C-(OH), and O-R species with R = $-CH_3$, $-CH_2CH_3$). On the other hand, the presence of the C 1s spectral counterpart of formate and C-(OH) (well discriminated in BE) allowed us to build up a consistent O 1s fitting. Therefore, although we cannot completely exclude the presence of surface Cu-OH, its concentration is most likely below the detection limit of the technique (about 0.02 ML). C-O bonds fall instead in the middle region, namely between 530.8 eV and 532.0 eV. Within this range, from lower to higher BE, we identify chemisorbed CO_2, C-O(H), and formate (HCOO−) overlapping at 530.8 eV; l-CO_2 at 531.4 eV; and carbonates at 531.8 eV (15, 25). Finally, at high BE we observed adsorbed H_2O (H_2O_{ads}) at 532.4 eV (15, 25).

The difficulty in discriminating between Cu^0 and Cu^+ using Cu core levels has been well established and is clearly evidenced from Fig. S5*A*, reporting the Cu 3p photoelectron spectra. To overcome this limitation, the various Cu surfaces were characterized by means of the Cu Auger $L_3M_{4,5}M_{4,5}$ transition and the valence band (VB) as described in *Discussion* and as reported in Figs. S5*B* and S6.

It is important to note that the BE of the aforementioned chemically shifted components for C 1s and O 1s do not change with the experimental conditions (within the spectral resolution, ∼0.15 eV), with an exception only for the adsorbed CO_2, where the adsorption configuration (b-CO_2 vs. l-CO_2) depends on the experimental conditions. In particular, we observe an important decrease by ∼0.50 eV (Fig. 2*B*) of the C 1s BE when CO_2 is codosed with H_2O on the metallic Cu(111) surface (Fig. S2). This work was inspired by similar experiments previously reported by Deng et al. (15), where they dosed CO_2 and H_2O separately and together on a polycrystalline (nonoriented) Cu sample. The authors observed the presence of an adsorbed CO_2 species at r.t. (with the corresponding C 1s centered at BE = 288.4 eV), which they labeled as a negatively charged adsorbed "$CO_2^{\delta-}$." We believe their adsorbed CO_2 species could actually be attributed to the l-CO_2 configuration observed and computed in this work. Interestingly, however, the authors did not observe a new component in the adsorbed CO_2 spectral region (287.9–288.5 eV, i.e., the b-CO_2), passing from the exposure to pure CO_2 to CO_2+ H_2O. In addition, we observe only a weak presence of reaction products between CO_2 and H_2O codosed at r.t. (Fig. 2 *C* and *D*), whereas Deng et al. (15) observed the significant development of the methoxy group spectral component ($-OCH_3$, BE = 285.2 eV) when codosing CO_2 and H_2O. These differences might be addressed by the higher experimental gas pressures used in this study, as well as potentially different investigated surface structures formed by different surface cleaning and annealing procedures. Overall, these differences can potentially lead to a different surface reactivity. The results reported by Deng et al. (15) have been obtained on a polycrystalline surface

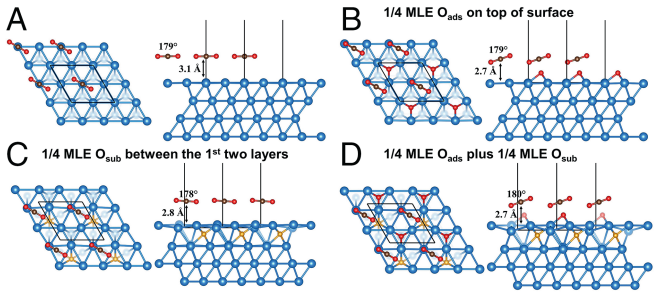

Fig. 3. Predicted structures for 1/4 ML of physisorbed *l*-CO_2 on various Cu surfaces (Cu, light blue; C, brown; O, red, but O_{sub} is marked in orange). (*A–D*) Top and side views of (*A*) pristine Cu(111), $\Delta G = +0.27$ eV, p_{thresh} = 33 atm; (*B*) Cu(111) with 1/4 ML O_{ads} (row 1 of Table 2) $\Delta G = +0.21$ eV, $p_{thresh} = 3$ atm; (*C*) Cu(111) with 1/4 ML O_{sub}, (row 2 of Table 2) $\Delta G = -0.39$ eV, $p_{thresh} = 2 \times 10^{-7}$ Torr; and (*D*) Cu(111) with 1/4 ML of both O_{ads} and O_{sub} (row 3 of Table 2), $\Delta G = -0.13$ eV, p_{thresh} = 7 Torr. Both *C* and case *D* are consistent with experiment.

likely exposing extended grain boundaries and coexistence of different surface orientations, whereas the present study was performed on an oriented surface. Our experimental results can be explained in terms of two different adsorption configurations of CO_2: (i) physisorbed linear CO_2 (*l*-CO_2) above 0.150 Torr (Fig. 3) stabilized by small amounts of residual O_{sub} and (ii) chemisorbed CO_2 (*b*-CO_2) that is formed only after adding H_2O, but also requires O_{sub}.

For pure CO_2 on pristine metallic Cu(111) (Fig. 2 *C* and *D*, experimental condition A), we observe experimentally a weakly adsorbed *l*-CO_2 at 298 K with a pressure of 0.7 Torr CO_2. This does not agree with our DFT calculations, performed at the M06L level, including the electron correlation required for London dispersion (vdW attraction) (16). We find an electronic binding energy of $\Delta E = -0.36$ eV and an enthalpy of binding of $\Delta H(298\ K) = -0.30$ eV [after including zero-point energy (ZPE) and specific heat]; however, due to the large decrease in entropy from the free CO_2 molecule, the free energy for *l*-CO_2 is uphill by $\Delta G(298\ K, 0.7\ Torr) = +0.27$ eV. These energetics would require pressures of 33 atm (~25 M Torr) for the adsorbed *l*-CO_2 to be observed at 298 K on pure metallic Cu(111). This is in line with previous experimental observations reported in the literature (also Fig. 1), where only *l*-CO_2 was observed on metallic Cu(111) surface at 298 K (7).

On the other hand, our DFT calculations show that very small amounts of suboxide (one suboxide O per every four surface Cu in our calculations, but likely much smaller levels are sufficient) lead to a negative free energy of $\Delta G(298\ K, 0.7\ Torr) = -0.12$ eV, which would stabilize physisorbed *l*-CO_2 at our experimental conditions. Indeed, our experiments find evidence for small amounts (~0.08 ML) of surface suboxide on our freshly prepared Cu(111) (Fig. 2*D*, experimental condition A). Such subsurface adsorbed O (denoted Cu-O_{sub}) has been observed often near the Cu surface, most likely resulting from oxygen impurities in the chamber (28) or partial dissociative adsorption of CO_2 (13). Interestingly, even if CO_2 is still in a linear configuration (similar to the gas phase), we observe experimentally that the O 1s and C 1s core-level BEs of *l*-CO_2 shift downward by ~4.9 eV compared with *g*-CO_2 (Fig. S4). This important shift means that an actual interaction is taking place between the adsorbate and the surface (7, 22), although the adsorption state still resembles physisorption.

To interpret these findings, we investigated in detail the influence of O_{sub} on the formation of *l*-CO_2, using various levels of DFT calculations. These calculations are discussed in detail in *Supporting Information*. It is well known that standard DFT methods [e.g., generalized gradient approximation (GGA) and local-density approximation (LDA)] do not account for London dispersion, which is usually included with empirical corrections (29). However, there is no rigorous basis for the empirical vdW correction for Cu. Instead we use the M06L version of DFT that includes both kinetic energy and exchange correlation functions optimized by comparing to a large benchmark of known vdW clusters with accurately known bonding energies (16). Further details are presented in *Computational Details of DFT Calculations*, Dataset S1, and Tables S1 and S2.

Table 2. DFT models of Cu(111) with various distributions of surface O atoms and of calculated O 1s BE with experimental APXPS results

Method	Structure	Predicted δO_{ads} and δO_{sub}
DFT	1/4 ML O_{ads}	$\delta O_{ads} = -2.2$ eV
DFT	1/4 ML O_{sub}	$\delta O_{sub} = -1.3$ eV
DFT	1/4 ML O_{ads} + 1/4 ML O_{sub}	$\delta O_{ads} = -0.3$ eV; $\delta O_{sub} = -1.5$ eV
APXPS	0.06 ML O_{ads} + 0.08 ML O_{sub}	$\delta O_{ads} = -0.4$ eV; $\delta O_{sub} = -1.6$ eV

Physisorbed CO_2 on Cu(111)

Fig. 3*A* shows the predicted surface structure for 1/4 monolayer (ML) equivalents (MLE) of CO_2 on metallic (O_{sub}-free) Cu(111). The physisorbed *l*-CO_2 molecules have a C-O bond distance of 1.164 Å compared with 1.163 Å in gas phase and O-C-O angles of 179°, with an equilibrium distance of 3.11 Å from the C atom of CO_2 to the Cu surface, characteristic of weak vdW interactions. The quantum mechanical (QM) electronic bond energy to the surface is $\Delta E = -0.36$ eV with $\Delta H(298\ K) = -0.30$ eV enthalpy of bonding (after including ZPE and specific heat). However, the large decrease in entropy from the free CO_2 molecule leads to a free energy for physisorbed CO_2 that is unfavorable by $\Delta G(298\ K, 0.7\ Torr) = +0.27$ eV, which would require a pressure of 33 atm to observe at 298 K.

Physisorbed CO_2 with O on Cu(111)

The experimentally observed O 1s shifts indicate a small amount of surface and/or subsurface adsorbed O (denoted O_{ads} and O_{sub}, respectively) is present in our pristine Cu(111). Compared with

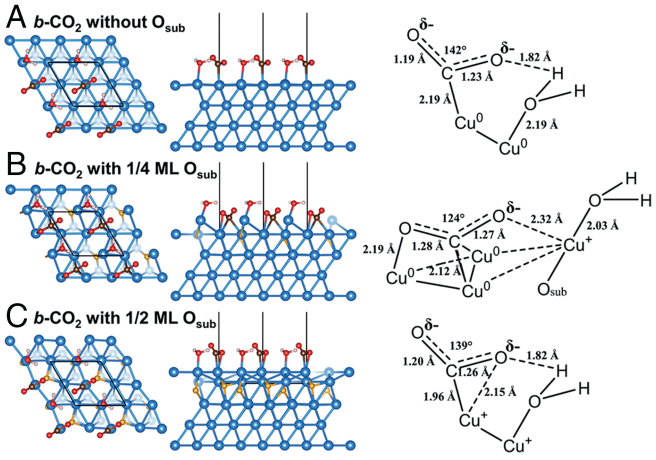

Fig. 4. M06L predicted structures for chemisorbed *b*-CO_2 with H_2O on Cu(111) with different levels of O_{sub}. ΔG is reported for 298 K, and $p = 0.35$ Torr for H_2O and CO_2. (*A–C*) Top and side views with chemical illustration of predicted structures (*A*) on pristine Cu(111), $\Delta G = +1.07$ eV; (*B*) on Cu(111) with 1/4 ML O_{sub}, $\Delta G = -0.06$ eV; and (*C*) on Cu(111) with 1/2 ML O_{sub}, $\Delta G = +0.28$ eV.

CHEMISTRY

the O 1s BE of O in the l-CO_2 configuration, we observe an experimental shift (δO_{ads}) of -0.4 eV for O_{ads} and an experimental shift (δO_{sub}) for O_{sub} of -1.6 eV. To deduce the nature of this O_{ads}, we consider the three cases reported in Table 2.

For computational convenience we assumed a 2×2 surface cell, but the experimental O_{sub} coverage is about 0.08 MLE. For the 2×2 unit cell, our DFT calculations find two cases with O 1s BE consistent with experiment. Fig. 3*C* with one O_{sub} per cell leads to a BE = -1.35 eV whereas Fig. 3*D* with one O_{sub} and one O_{ads} leads to BE = 0.31 and 1.54 eV. Referencing to gas-phase O_2 (standard conditions), Fig. 3*D* is $\Delta G = -2.34$ eV more stable than Fig. 3*C*. For case Fig. 3*C* we predict $\Delta G = -0.39$ eV bonding for l-CO_2 (a pressure threshold of 2×10^{-7} Torr), whereas Fig. 3*D* leads to $\Delta G = -0.13$ eV with a pressure threshold of 7 Torr, both consistent with experiment.

Simultaneous dosing of CO_2 in the presence of $H_2\mathbf{O}$ leads to a dramatic change in the character of the surface CO_2, showing clearly the adsorption characteristics for chemisorbed b-CO_2. For a Cu(111) surface that includes some surface suboxide, the DFT calculations lead to several local minima (Fig. 4): (*i*) physisorbed l-CO_2 plus H_2O_{ad}, (*ii*) chemisorbed b-CO_2 plus H_2O_{ads} (Fig. 4 *A*–*C*), (*iii*) reacted $COOH_{ads}$ plus OH_{ads} (Fig. S7*A*), and (*iv*) HCOOH plus surface O_{ads} (Fig. S7*B*).

In the case of Cu(111) without O_{sub} (Fig. 4*A*), the C atom of b-CO_2 is chemically bonded to a surface Cu^0, whereas the two O atoms accommodate the partial negative charge transferred from the Cu surface, with one stabilized by hydrogen bonding to H_2O_{ad}. However, this b-CO_2 leads to a QM binding energy of $\Delta E = -0.23$ eV, but including vibrational and entropy contributions we find b-CO_2 is unstable, with ΔG(298 K, 0.7 Torr) = 1.07 eV, which agrees with our experiments.

When the O_{sub} is increased to 1/4 ML (Fig. 4*B*), we find that the C atom is chemically bonded to two surface Cu^0, one O atom is chemically bonded to one Cu^0 center, and the other O atom is stabilized by the surface Cu^+ pulled up by H_2O_{ad}. This b-CO_2 leads to ΔG(298 K, 0.7 Torr) = -0.06 eV, which is stable in agreement with our experiments.

However, increasing the O_{sub} to 1/2 ML, we predict that ΔG(298 K, 0.7 Torr) = $+0.28$ eV, which is unstable. Here the C atom is chemically bonded to a surface Cu^+ that shares an O atom bearing a partial charge (stabilized by a hydrogen bonding to H_2O_{ad} on surface Cu^+). Our experiments also show that increased levels of O_{sub} decrease the binding of b-CO_2. Thus, we find that chemisorbed b-CO_2 is stable only for the case in Fig. 4*B* with 1/4 ML O_{sub}. Having more O_{sub} or none at all destabilizes b-CO_2. We explain this in terms of the distinct interactions of Cu^0 and Cu^+ induced by the $Cu(111)O_{sub,x=0.25}$.

This result of an optimum O_{sub} for b-CO_2 is in agreement with our experiments for CO_2 and H_2O codosing on the $Cu_{x=2.5}O$ and $Cu_{x=1.5}O$ suboxide structures, which shows both b-CO_2 and l-CO_2, but with a l-CO_2/b-CO_2 ratio of 3.8 and 5.3 for $Cu_{x=2.5}O$ to the $Cu_{x=1.5}O$ structure, respectively (the ratio was determined from both C 1s and O 1s spectra) (Fig. S3 *A* and *B*). In addition, Fig. S8 reports the experimental results of exposing the $Cu_{x=1.5}O$ structure to 0.7 Torr of 1:1 CO_2 and O_2. In this case we do not observe chemisorbed b-CO_2, but only physisorbed l-CO_2 and its conversion to surface $-CO_3$ (carbonate).

The DFT calculations predict that on $Cu(111)O_{sub,x=0.25}$, b-CO_2 can react with H_2O_{ad} to form formate plus OH_{ads}, but the product is unstable in our conditions, with ΔG(298 K, 0.7 Torr) = $+0.20$ eV, making it endothermic from b-CO_2 in Fig. 4*B* by ΔG(298 K, 0.7 Torr) = 0.26 eV [it is 0.43 eV endothermic for $Cu(111)O_{sub,x=0.5}$]. On the other hand, our DFT calculations predict that this formate can extract an H from the $-OH$ to form formic acid plus O_{ads}, which is stable with ΔG(298 K, 0.7 Torr) = -0.05.

We expect that learning how to tune the character of the surface atoms (Cu^0 vs. Cu^+ in this case) to manipulate these relative energetics of l-CO_2 plus H_2O, b-CO_2 plus H_2O, formate plus OH, and formic acid plus O_{ads} may allow us to design modified systems aimed at accelerating these reaction steps. For example, we hypothesize that other subsurface anions such as S or Cl might favorably modify the energetics by changing the charges and character of the surface atoms and/or replacing some Cu with Ag, Au, or Ni with different redox properties.

Activation of the inert linear l-CO_2 molecule requires enforcing a bent b-CO_2 configuration (30) with great chemical stabilization, but pristine Cu(111) and corresponding derivatives with O_{sub} and/or O_{ads} do not deliver sufficient stabilization, as shown in our calculations. Thus, forcing CO_2 to have the necessary angle ($120° \sim 140°$) and appropriate distance (~ 2 Å) to the pristine Cu surface, we find no stable local minimum; all of the initial bent CO_2 structures relax into the stable l-CO_2 physisorption state.

However, the presence of modest amounts of O_{sub} generates a mixture of surface Cu^+ and Cu^0 atoms that combines with H_2O_{ad} to stabilize the b-CO_2 structure reported in Fig. 4*B*. We conclude that this configuration of surface atoms and H_2O is responsible for stabilizing b-CO_2 and opening up the possibility of forming formate, formic acid, etc. This elucidates the first reduction step of CO_2.

This combination of APXPS experiments and DFT calculations enabled us to obtain a detailed understanding of the initial steps of CO_2 activation by H_2O on a Cu surface. We find that a modest level of O_{sub} between the top two Cu layers is essential for stabilizing physisorbed l-CO_2.

This unexpected finding may explain a general observation empirically derived in the literature from the catalytic performance of Cu oxides for CO_2RR: It is known that Cu catalysts previously treated to generate surface oxides generally show improved activity compared with the pristine metallic surface (3, 6, 31). From our experimental results and theoretical predictions, we conclude that the topmost layer needs to expose metallic centers, because CO_2 can efficiently chemisorb only on such centers (Fig. 4*B*), to form the activated molecular substrate for subsequent reduction to formate and other products. However, we find that the presence of a subsurface oxide structure is also needed to promote H_2O chemisorption onto a Cu^+ center. This enables the electronic communication between adsorbed CO_2 and H_2O, favoring the transition from a linearly physisorbed l-CO_2 to a bent chemisorbed b-CO_2. From Fig. 4*B*, reactions to form formate and formic acid are possible but not favored under our conditions.

These results provide the insight that subsurface oxide plays a critical role in the initial steps for activating CO_2, providing a foundation for the rational development of unique active electrocatalysts.

ACKNOWLEDGMENTS. This work was supported through the Office of Science, Office of Basic Energy Science (BES), of the US Department of Energy (DOE) under Award DE-SC0004993 to the Joint Center for Artificial Photosynthesis and as part of the Joint Center for Energy Storage Research, DOE Energy Innovation Hubs. The Advanced Light Source is supported by the Director, Office of Science, Office of BES, of the US DOE under Contract DE-AC02-05CH11231. The QM calculations were carried out on the Zwicky supercomputer at Caltech.

1. Lewis NS, Nocera DG (2006) Powering the planet: Chemical challenges in solar energy utilization. *Proc Natl Acad Sci USA* 103:15729–15735.
2. Kuhl KP, Cave ER, Abram DN, Jaramillo TF (2012) New insights into the electrochemical reduction of carbon dioxide on metallic copper surfaces. *Energ Environ Sci* 5:7050–7059.
3. Li CW, Kanan MW (2012) CO_2 reduction at low overpotential on Cu electrodes resulting from the reduction of thick Cu_2O films. *J Am Chem Soc* 134:7231–7234.
4. Knop-Gericke A, Hävecker M, Schedel-Niedrig T, Schlögl R (2001) Characterisation of active phases of a copper catalyst for methanol oxidation under reaction conditions: An in situ x-ray absorption spectroscopy study in the soft energy range. *Top Catal* 15:27–34.

5. Qiao J, Liu Y, Hong F, Zhang J (2014) A review of catalysts for the electroreduction of carbon dioxide to produce low-carbon fuels. *Chem Soc Rev* 43:631–675.
6. Mistry H, et al. (2016) Highly selective plasma-activated copper catalysts for carbon dioxide reduction to ethylene. *Nat Commun* 7:12123.
7. Freund HJ, Roberts M (1996) Surface chemistry of carbon dioxide. *Surf Sci Rep* 25: 225–273.
8. Wurth W, et al. (1990) Bonding, structure, and magnetism of physisorbed and chemisorbed O_2 on Pt(111). *Phys Rev Lett* 65:2426–2429.
9. Rasmussen P, Taylor P, Chorkendorff I (1992) The interaction of carbon dioxide with Cu(100). *Surf Sci* 269:352–359.
10. Campbell CT, Daube KA, White J (1987) Cu/ZnO_x and ZnO_x/Cu(111): Model catalysts for methanol synthesis. *Surf Sci* 182:458–476.
11. Pohl M, Otto A (1998) Adsorption and reaction of carbon dioxide on pure and alkali-metal promoted cold-deposited copper films. *Surf Sci* 406:125–137.
12. Nakamura J, Rodriguez JA, Campbell CT (1989) Does CO_2 dissociatively adsorb on cu surfaces? *J Phys Condens Matter* 1:SB149–SB160.
13. Eren B, Weatherup RS, Liakakos N, Somorjai GA, Salmeron M (2016) Dissociative carbon dioxide adsorption and morphological changes on Cu(100) and Cu(111) at ambient pressures. *J Am Chem Soc* 138:8207–8211.
14. Fu SS, Somorjai GA (1992) Interactions of O_2, CO, CO_2, and D_2 with the stepped Cu(311) crystal face: Comparison to Cu(110). *Surf Sci* 262:68–76.
15. Deng X, et al. (2008) Surface chemistry of Cu in the presence of CO_2 and H_2O. *Langmuir* 24:9474–9478.
16. Zhao Y, Truhlar DG (2006) A new local density functional for main-group thermochemistry, transition metal bonding, thermochemical kinetics, and noncovalent interactions. *J Chem Phys* 125:194101.
17. Cattelan M, et al. (2013) Microscopic view on a chemical vapor deposition route to boron-doped graphene nanostructures. *Chem Mater* 25:1490–1495.
18. Schedel-Niedrig T, et al. (2000) Copper (sub)oxide formation: A surface sensitive characterization of model catalysts. *Phys Chem Chem Phys* 2:2407–2417.
19. Salmeron M, Schlögl R (2008) Ambient pressure photoelectron spectroscopy: A new tool for surface science and nanotechnology. *Surf Sci Rep* 63:169–199.
20. Starr DE, Liu Z, Hävecker M, Knop-Gericke A, Bluhm H (2013) Investigation of solid/vapor interfaces using ambient pressure X-ray photoelectron spectroscopy. *Chem Soc Rev* 42:5833–5857.
21. Grass ME, et al. (2010) New ambient pressure photoemission endstation at Advanced Light Source beamline 9.3.2. *Rev Sci Inst* 81:053106.
22. Browne V, et al. (1991) Activation of carbon dioxide at bismuth, gold and copper surfaces. *Appl Surf Sci* 47:375–379.
23. Sterrer M, et al. (2007) Control of the charge state of metal atoms on thin MgO films. *Phys Rev Lett* 98:096107.
24. Starr DE, Weis C, Yamamoto S, Nilsson A, Bluhm H (2009) NO_2 adsorption on Ag(100) supported MgO(100) thin films: Controlling the adsorption state with film thickness. *J Phys Chem C* 113:7355–7363.
25. Eren B, Heine C, Bluhm H, Somorjai GA, Salmeron M (2015) Catalyst chemical state during CO oxidation reaction on Cu(111) studied with ambient-pressure X-ray photoelectron spectroscopy and near edge X-ray adsorption fine structure spectroscopy. *J Am Chem Soc* 137:11186–11190.
26. Eren B, et al. (2016) Activation of Cu(111) surface by decomposition into nanoclusters driven by CO adsorption. *Science* 351:475–478.
27. Bluhm H, et al. (2004) Methanol oxidation on a copper catalyst investigated using *in situ* X-ray photoelectron spectroscopy. *J Phys Chem B* 108:14340–14347.
28. Spitzer A, Lüth H (1982) The adsorption of oxygen on copper surfaces: II. Cu(111). *Surf Sci* 118:136–144.
29. Grimme S, Antony J, Ehrlich S, Krieg H (2010) A consistent and accurate *ab initio* parametrization of density functional dispersion correction (DFT-D) for the 94 elements H-Pu. *J Chem Phys* 132:154104.
30. Spielfiedel A, et al. (1992) Bent valence excited states of CO_2. *J Chem Phys* 97: 8382–8388.
31. Kas R, et al. (2014) Electrochemical CO_2 reduction on Cu_2O-derived copper nanoparticles: Controlling the catalytic selectivity of hydrocarbons. *Phys Chem Chem Phys* 16:12194–12201.
32. Tougaard S (1989) Practical algorithm for background subtraction. *Surf Sci* 216: 343–360.
33. Evans S (1991) Curve synthesis and optimization procedures for X-ray photoelectron spectroscopy. *Surf Interface Anal* 17:85–93.
34. Muñoz-Flores J, Herrera-Gomez A (2012) Resolving overlapping peaks in {ARXPS} data: The effect of noise and fitting method. *J Electron Spectrosc Relat Phenom* 184:533–541.
35. Barman SR, Sarma DD (1992) Investigation of the L_3-$M_{45}M_{45}$ Auger spectra of Cu, Cu_2O and CuO. *J Phys Condens Matter* 4:7607–7616.
36. Pauly N, Tougaard S, Yubero F (2014) LMM Auger primary excitation spectra of copper. *Surf Sci* 630:294–299.
37. Tougaard S, Yubero F (2012) Software package to calculate the effects of the core hole and surface excitations on XPS and AES. *Surf Interface Anal* 44:1114–1118.
38. Simonsen AC, Yubero F, Tougaard S (1997) Quantitative model of electron energy loss in XPS. *Phys Rev B* 56:1612–1619.
39. Yubero F, Tougaard S (2005) Quantification of plasmon excitations in core-level photoemission. *Phys Rev B* 71:045414.
40. Dovesi R, et al. (2014) CRYSTAL14: A program for the *ab initio* investigation of crystalline solids. *Int J Quantum Chem* 114:1287–1317.
41. Stevens WJ, Krauss M, Basch H, Jasien PG (1992) Relativistic compact effective potentials and efficient, shared-exponent basis sets for the third-, fourth-, and fifth-row atoms. *Can J Chem* 70:612–630.
42. Favaro M, et al. (2016) A synchrotron-based spectroscopic study of the electronic structure of N-doped HOPG and PdY/N-doped HOPG. *Surf Sci* 646:132–139.
43. Favaro M, et al. (2015) *In situ* carbon doping of TiO_2 nanotubes via anodization in graphene oxide quantum dot containing electrolyte and carburization to TiO_xC_y nanotubes. *Adv Mater Interfaces* 2:1400462.
44. Schimka L, Harl J, Kresse G (2011) Improved hybrid functional for solids: The HSEsol functional. *J Chem Phys* 134:024116.
45. Heit YN, Nanda KD, Beran GJO (2016) Predicting finite-temperature properties of crystalline carbon dioxide from first principles with quantitative accuracy. *Chem Sci* 7:246.